Analyzing single-bond experiments: Influence of the shape of the energy landscape and universal law between the width, depth, and force spectrum of the bond

Julien Husson* and Frédéric Pincet†

Laboratoire de Physique Statistique de l'Ecole Normale Supérieure, Associé aux Universités Paris 6 et Paris 7, UMR CNRS 8550, 24 Rue Lhomond, 75231 Paris Cedex 05, France

(Received 13 June 2007; revised manuscript received 5 September 2007; published 14 February 2008)

Experimentalists who measure the rupture force of a single molecular bond usually pull on that bond at a constant speed, keeping the loading rate $r=\frac{df}{dt}$ constant. The challenge is to extract the energy landscape of the interaction between the two molecules involved from the experimental rupture force distribution under several loading rates. This analysis requires the use of a model for the shape of this energy landscape. Several barriers can compose the landscape, though molecular bonds with a single barrier are often observed. The Bell model is commonly used for the analysis of rupture force measurements with bonds displaying a single barrier. It provides an analytical expression of the most likely rupture force which makes it very simple to use. However, in principle, it can only be applied to landscapes with *extrema* whose positions do not vary under force. Here, we evaluate the general relevance of the Bell model by comparing it with another analytical model for which the landscape is harmonic in the vicinity of its *extrema*. Similar shapes of force distributions are obtained with both models, making it difficult to confirm the validity of the Bell model for a given set of experimental data. Nevertheless, we show that the analysis of rupture force experiments on such harmonic landscapes with the Bell model provides excellent results in most cases. However, numerical computation of the distributions of the rupture forces on piecewise-linear energy landscapes indicates that the blind use of any model such as the Bell model may be risky, since there often exist several landscapes compatible with a given set of experimental data. Finally, we derive a universal relation between the range and energy of the bond and the force spectrum. This relation does not depend on the shape of the energy landscape and can thus be used to characterize unambiguously any one-barrier landscape from experiments. All the results are illustrated with the streptavidin-biotin bond.

DOI: 10.1103/PhysRevE.77.026108 PACS number(s): 82.20.Db, 82.37.Gk, 05.10.Gg, 68.47.Pe

I. INTRODUCTION

The cohesion of any type of biological matter is ensured by covalent and noncovalent bonds. The first ones are responsible for the cohesion of the backbone of biomolecular structures while the second ones are intrinsically transient and provide the various mechanical and dynamic properties of biological objects. In recent years, many have undertaken the challenge of probing single noncovalent molecular bonds. Many such bonds have been investigated by means of flow chambers [1,2], atomic force microscopes [3,4], biomembrane force probes [5–8], optical tweezers [9,10], and other techniques [11].

One of the difficulties in measuring the rupture forces of single molecular bonds is that, unlike macroscopic adhesions, they are very sensitive to thermal fluctuations. Therefore only a distribution of rupture forces can be obtained for each measurement condition. The simplest experimental conditions consist of disrupting a bond by pulling on it with a spring at a constant speed. The bond is thus submitted to an external force that increases at a constant rate r, also called the loading rate. The external force f at time t is then $f=rt$. The analysis of the rupture-force distributions at different loading rates makes it possible to extract intrinsic properties of the bond. However, this analysis requires a model for the dynamics of the bond.

It is commonly agreed that these dynamics are well-described by models inspired from Kramers' theory [12,13]. In that scheme, the bond is approximated by a one-dimensional energy landscape in which the two bound molecules are trapped. During the separation process at a specific loading rate, the energy landscape is tilted by the increasing pulling force [14]. At any given time, the dynamics of the bond can be equivalently described by Langevin or by Smoluchowski equations, and formation as well as dissociation rates can be computed between successive metastable states [15]. Consequently, this theory allows a direct deduction of the rupture-force distribution when the energy landscape of the bond is known. More precisely, in order to apply Kramers' theory, one needs to know the height and curvature of any *extremum* in the landscape for any given pulling force exerted on the bond. Experimentalists have to go the other way around by deducing the energy landscape from the measured distributions of rupture forces. While it is clearly impossible to accurately obtain the overall energy landscape, its main features can nonetheless be extracted. For this purpose, a shape of the energy landscape has to be assumed.

In this paper, we focus on the case where the energy landscape under zero force displays a single barrier with a given height and position. We discuss the influence of the shape of the landscape on the analysis of rupture-force experiments.

*Present address: Foundation for Fundamental Research on Matter (FOM) Institute for Atomic and Molecular Physics (AMOLF), Kruislaan 407, 1098 SJ Amsterdam, The Netherlands. j.husson@amolf.nl

†Corresponding author. pincet@lps.ens.fr

First (Sec. II), we describe the well-known model introduced by Bell [16], which was adapted by Evans [15] for the case of rupture-force measurements. We introduce another model, the harmonic model, in which we postulate a shape of the energy landscape that enables us, like in the Bell model, to analytically solve the time evolution equation of the system. We compare the solution of this equation obtained with both models, and show that, by analyzing rupture-force measurements, one deduces parameters defining the energy landscape, i.e., the height and the position of the barrier, which depend on the chosen model. Nevertheless, both models lead to parameters sufficiently close to claim that their predictive power is comparable. Hence we conclude that in general, the simplest model, i.e., the Bell model, should be used for the analysis of rupture-force experiments.

One could also hope to deduce the whole shape of the landscape from the experimental data. Unfortunately, we also predict that whatever the analyzed data is, it is almost impossible to experimentally differentiate between different types of landscape shapes from rupture-force measurements. This means that one can only hope to obtain the height and the position of the barrier but not the detailed shape of the energy landscape.

Finally, since these two models do not describe all the possible shapes of energy landscape, we broadened our study by numerically solving the time evolution equation applied on a piecewise-linear energy landscape. Such landscape provides a good approximation of any one-barrier landscape (Sec. III). Even though rupture force distributions display a great diversity—and within this diversity several cases where both the Bell and the harmonic models break down—their analysis leads to a "universal" law relating the force spectrum to the height and the position of the barrier. This relation can be used to characterize unambiguously any one-barrier energy landscape from experiments. All these results are applied to experimental data obtained on the well-known streptavidin-biotin bond [8].

II. TWO MODELS LEADING TO ANALYTICAL SOLUTIONS OF THE TIME EVOLUTION EQUATION

A. Notations

In this paper we consider a one-dimensional energy landscape $E(x)$ of the bond where x is the reaction coordinate during the rupture of the bond. In the absence of any applied force, $E(x)$ exhibits a minimum (zero-valued by convenience) at $x=0$ and a maximum at $x=x_b$: $E(0)=0$ and $E(x_b)=E_b>0$. Under an applied force f, the energy landscape is tilted so that the energy becomes $E(x)-fx$. This energy has a minimum located at $x_m(f)$ and a maximum located at $x_b(f)$; $x_m(f)$ and $x_b(f)$ depend *a priori* on the applied force. We call, respectively, $\Delta E(f)$, $\Delta x(f)=x_b(f)-x_m(f)$, $\kappa_m(f)$, and $\kappa_b(f)$ the positive energy difference between the barrier and the minimum, the positive distance between the barrier and the minimum, the curvature near the minimum and the curvature near the barrier (in $\mathrm{pN\,nm^{-1}}$). Following these definitions: $\Delta E(f)=[E(x_b(f))-fx_b(f)]-[E(x_m(f))-fx_m(f)]$, so that $\Delta E(f)=E(x_b(f))-E(x_m(f))-f\Delta x(f)$.

Finally, when the applied force is larger than the largest slope of the landscape, the resulting tilted landscape is continuously decreasing, meaning that there is no more barrier to pass for the bond to dissociate. This largest slope of the landscape is called the critical force.

B. Master equation

In a widely used approach for modeling the dynamics of a single bond submitted to a constant loading rate r (i.e., $f=rt$) [15], the probability $P(f)$ for the bond to remain intact under an applied force f follows the time evolution equation, or master equation:

$$\frac{dP(f)}{df} = -\frac{k_{off}(f)}{r}P(f), \tag{1}$$

where $k_{off}(f)$ (expressed in $\mathrm{s^{-1}}$) is the off-rate, or rate of rupture of a single bond under an applied force f. We point out that in this model any rebinding events after dissociation are neglected, following the assumption made by Evans in Ref. [14]. Rebinding events are very rare because, when a force is applied, it tilts the landscape, which pushes the molecules to separate quickly far away once the top of the barrier is reached. Other authors [17,18] investigated the influence of these rebinding events.

Furthermore, $k_{off}(f)$ can be written as

$$k_{off}(f) = \frac{1}{t_D(f)}\exp\left(-\frac{\Delta E(f)}{k_BT}\right), \tag{2}$$

where $t_D(f)$ is the inverse attempt frequency. Equation (2) shows that the same $k_{off}(f)$ can be obtained by a simultaneous shift in $t_D(f)$ and $\Delta E(f)$. Applying Kramers' theory [12,13], one can write

$$t_D(f) = \frac{2\pi\zeta}{\sqrt{\kappa_m(f)\kappa_b(f)}}. \tag{3}$$

Here, ζ is the damping coefficient which stands in the range $(2-5)\times 10^{-8}$ $\mathrm{pN\,s\,nm^{-1}}$ and is dependent on the effective viscosity of the surrounding medium [15,19–21] and possible hydrodynamic effects. The distribution of the rupture force, or the probability density, $p(f)$ (expressed in $\mathrm{pN^{-1}}$) is given by

$$p(f) = -\frac{dP(f)}{df}. \tag{4}$$

By definition, $p(f)df$ is the probability that the bond will break between forces f and $f+df$.

When the shape of the energy landscape—which appears through the explicit expression of $\Delta E(f)$, $\kappa_m(f)$, and $\kappa_b(f)$—and ζ are known, Eqs. (1)–(4) are sufficient for deducing a general expression for $p(f)$:

$$p(f) = \frac{k_{off}(f)}{r}\exp\left(-\int_0^f \frac{k_{off}(\alpha)}{r}d\alpha\right). \tag{5}$$

In order to obtain an analytical expression of $p(f)$, the integral in Eq. (5) has to be computed. According to Kramers'

theory, Eqs. (1)–(5) are only valid for f corresponding to $\Delta E(f)$ which are larger than the thermal energy k_BT.

C. Force spectrum and nondimensional variables

When the loading rate r is sufficiently high, $p(f)$ possesses a maximum at f^* which increases with r. f^* is the most likely rupture force. The differentiation of Eq. (5) gives (see Refs. [22,23] for other similar derivations)

$$2\ln(k_{off}(f^*)) = \ln(r) + \ln\left(\frac{dk_{off}}{df}(f^*)\right). \tag{6}$$

In all the models considered in this paper, t_D will not depend on f. It is then convenient to use dimensionless variables for f^*, ΔE, r, and $p(f)$, noted $\tilde{f}^*$, $\Delta\tilde{E}$ (and $\tilde{E}_b$), $\tilde{r}$, and $\tilde{p}(\tilde{f})$, respectively. We define those variable as follows: $\tilde{f}=\frac{f}{E_b/x_b}$, $\tilde{E}_b=\frac{E_b}{k_BT}$, $\tilde{r}=\frac{r}{E_b/x_bt_D}$, and $\tilde{p}(\tilde{f})=\frac{E_b}{x_b}p\left(\frac{E_b}{x_b}\tilde{f}\right)$. Further below, nondimensional variables will always be written with the superscript $\tilde{}$. With these variables, Eq. (6) becomes

$$\ln(\tilde{r}) + \ln\left(-\frac{d\Delta E}{d\tilde{f}}(\tilde{f}^*)\right) + \Delta\tilde{E}(\tilde{f}^*) = 0. \tag{7}$$

The plot of f^* vs $\ln r$ is called the force spectrum of the bond (as introduced in the dynamic force spectroscopy theory [24]).

D. Bell model

The most commonly used model for analyzing single-molecule force measurements has been introduced in the seminal work by Bell [16], and further developed by Evans [15]. It essentially makes two implicit assumptions: (i) the relative position of the barrier and minimum of the energy landscape is constant during the bond rupture process; and (ii) $t_D(f)$ has to be imposed since the curvatures are not defined and $t_D(f)$ does not vary with f. In this case, $k_{off}(f)=\frac{1}{t_D}\exp\left(-\frac{E_b-fx_b}{k_BT}\right)$; $p(f)$ can be derived analytically from Eq. (5) and one obtains

$$p(f) = \frac{\exp\left(\frac{-E_b}{k_BT}\right)}{t_Dr}\exp\left(\frac{fxb}{k_BT} + \frac{k_BT\exp\left(\frac{-E_b}{k_BT}\right)}{x_bt_Dr}\times\left[1-\exp\left(\frac{fx_b}{k_BT}\right)\right]\right). \tag{8}$$

It is worth noting that for the Bell model to be valid at all forces where Eqs. (1)–(5) hold, the landscape is implicitly completely equivalent to a linear increasing function of the reaction coordinate x, so that the *extrema*'s locations are independent of the force.

We will not discuss other approaches based on reconstruction methods that use Jarzynsky's equality [25–27], nor other analysis that include the energy landscape's roughness [28]. Furthermore, in this paper we only treat the case of so-called slip bonds, for which the off-rate is an increasing function of the applied force. When studying other types of specific bonds, like catch bonds, for which the off-rate is a nonmonotonous function of the applied force, other groups [5,29–32] have used multiple-pathways dissociation schemes, or different one-dimensional (1D) models (see Ref. [33], where a description of recent models for catch bonds can also be found), which we do not consider here. Finally, other approaches on slip bonds are discussed in Ref. [34].

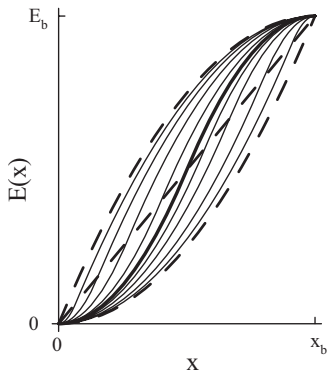

FIG. 1. Plot of the energy landscapes $E(x)$ (under zero force) vs the reaction coordinate x, for a given barrier position x_b and a given barrier height E_b. The solid lines represent the energy landscapes treated by the harmonic model. Two parabolas (dashed curves) limit these possible energy landscapes. The thick solid line represents the landscape obtained when the curvatures at the minimum and at the top of the energy barrier are equal: $\kappa_m=\kappa_b=\frac{4E_b}{x_b^2}$. The straight dashed line represents a landscape that corresponds to the Bell model.

E. Harmonic model

Other shapes of energy landscapes have been considered in the large number of single-bond force measurements studies, e.g., a minimum given by a harmonic potential [33,35]. However, analytical expressions of the rupture force distributions are rarely found in literature, although some interesting results have been obtained in Refs. [17–19,36,37] and very recently in Refs. [38,39]. Here, we propose a shape that combines the advantages of giving a full analytical description and representing a large panel of energy landscapes. In this model, the potential is supposed to be harmonic in the vicinity of both the minimum and the barrier. In other terms:

$$E(x) = \frac{1}{2}\kappa_m x^2 \;\forall\, x, \quad 0 \leqslant x \leqslant x_c,$$

$$E(x) = E_b - \frac{1}{2}\kappa_b(x-x_b)^2 \;\forall\, x, \quad x_c \leqslant x \leqslant x_b, \tag{9}$$

where x_c is the location where the two harmonic components are tangentially connected [i.e., $\frac{dE}{dx}(x)$ is continuous; Fig. 1 shows examples of such landscapes]. The curvatures κ_m and κ_b are independent of the force (hence the force-independent notations). Equation (3) shows that, like in the Bell model, the inverse attempt frequency $t_D(f)$ does not depend on f. Because of the tangential connection at $x=x_c$, the curvatures are linked by

$$\frac{\kappa_m \kappa_b}{\kappa_m + \kappa_b} = \frac{2E_b}{x_b^2}. \tag{10}$$

$\Delta E(f)$ is then independent of the curvatures:

$$\Delta E(f) = \frac{\left(E_b - \frac{fx_b}{2}\right)^2}{E_b}. \tag{11}$$

As a result, given a certain height and position of the barrier, all the energy landscapes presented in Fig. 1 can be treated simultaneously [only t_D is different, following Eq. (3)]. These energy landscapes correspond to a curvature κ_m varying from $\frac{2E_b}{x_b^2}$ to infinity, whereas in accordance with Eq. (10), κ_b varies from infinity down to $\frac{2E_b}{x_b^2}$. Out of this range, a tangential connection between both harmonic potentials around the minimum and the top of the barrier is not possible. For a value of κ_b approaching infinity, our model brings us back to energy landscape shapes similar to those studied in Refs. [36,37]. In the other limiting case, we describe a barrier with a cusp placed at the minimum, and a harmonic potential around the barrier.

The advantage of the tangential connection between both harmonic potentials is that it allows the simultaneous treatment of the whole family of smooth landscapes shown in Fig. 1 and leads to analytic solutions for $k_{off}(f)$ and $p(f)$ from Eqs. (2), (5), and (11):

$$k_{off}(f) = \frac{1}{t_D} \exp\left[-\left(\frac{E_b - \frac{fx_b}{2}}{\sqrt{k_B T E_b}}\right)^2\right], \tag{12}$$

$$p(f) = \frac{1}{rt_D} \exp\left\{-\left(\frac{E_b - \frac{fx_b}{2}}{\sqrt{k_B T E_b}}\right)^2 + \frac{\sqrt{\pi k_B T E_b}}{rt_D x_b} \times \left[\operatorname{erf}\left(\frac{E_b - \frac{fx_b}{2}}{\sqrt{k_B T E_b}}\right) - \operatorname{erf}\left(\frac{E_b}{\sqrt{k_B T E_b}}\right)\right]\right\}, \tag{13}$$

where the error function erf is defined as

$$\operatorname{erf}(x) = \frac{2}{\sqrt{\pi}} \int_0^x \exp(-z^2) dz.$$

Note that the harmonic model reduces to the Bell model (with t_D which is fully determined by the shape of the landscape) when the force is sufficiently small. Quantitatively, this occurs when the second order term in Eq. (11) can be neglected against the first order one, i.e., for $\frac{fx_b}{4E_b} < 0.1$. For $x_b = 0.5$ nm, $E_b = 20 k_B T$ this corresponds to $f < 16$ pN.

F. Comparison of the force spectrum of the Bell and harmonic models

The most likely rupture force f^* can be deduced from Eq. (6) for both models. In the case of the Bell model, it has long been recognized [24] that f^* varies linearly with $\ln r$ according to

$$f^* = \frac{k_B T}{x_b}\left[\ln\left(\frac{rt_D x_b}{k_B T}\right) + \frac{E_b}{k_B T}\right]. \tag{14}$$

Therefore the force spectrum is a straight line that provides a complete description of the energy landscape: the position and height of the barrier are deduced from the slope and the value of f^* for $\ln\left(\frac{rt_D x_b}{k_B T}\right) = 0$, respectively, provided that t_D is known. For dimensionless variables, Eq. (14) becomes

$$\tilde{f}^* = \frac{1}{\tilde{E}_b} \ln \tilde{r} + \left(1 + \frac{\ln \tilde{E}_b}{\tilde{E}_b}\right). \tag{15}$$

For the harmonic model, f^* is given by

$$f^* = \frac{2E_b}{x_b}\left(1 - \sqrt{\frac{k_B T \operatorname{plog}\left(\frac{2E_b k_B T}{(x_b t_D r)^2}\right)}{2E_b}}\right), \tag{16}$$

where $\operatorname{plog}(\alpha)$ is the product logarithm, the solution of equation $\alpha = \operatorname{plog}(\alpha)\exp[\operatorname{plog}(\alpha)]$. Equation (16) can be rewritten as

$$\tilde{f}^* = 2\left(1 - \sqrt{\frac{\operatorname{plog}\left(\frac{2}{\tilde{r}^2 \tilde{E}_b}\right)}{2\tilde{E}_b}}\right). \tag{17}$$

For a given x_b, the Bell and the harmonic models predict different values for f^*, and this difference is a function of E_b. We also note that the expression of $\tilde{f}^*$ given by the harmonic model, i.e., Eq. (17), can be approximated by a more explicit expression $\tilde{f}^* \approx 2\left(1 - \frac{-1+\sqrt{1-4\tilde{E}_b(\ln \tilde{r} + \ln \tilde{E}_b - 1)}}{2\tilde{E}_b}\right)$ which is, as Eq. (17), a nonlinear function of $\ln \tilde{r}$ [in opposition to Eq. (15)]. As a consequence, it could seem possible to distinguish the two models from the experimental data. However, technical limitations in the experimental setups currently used make it a lot more complicated. The accessible loading rates cover six orders of magnitude: from 0.1 pN/s to 0.1 μN/s. The normalizing factor for the loading rates, $\frac{E_b}{x_b t_D}$, will always be bounded by values whose order of magnitude is $\frac{E_b}{x_b t_D} = \frac{35 k_B T}{0.1\ \text{nm} \times 10^{-11}\ \text{s}} \approx 10^{14}$ pN/s and $\frac{E_b}{x_b t_D} = \frac{10 k_B T}{3\ \text{nm} \times 10^{-9}\ \text{s}} \approx 10^{10}$ pN/s, so that $\tilde{r}$ can vary between $\tilde{r} = \frac{0.1\ \text{pN/s}}{10^{14}\ \text{pN/s}} = 10^{-15}$ and $\tilde{r} = \frac{10^5\ \text{pN/s}}{10^{10}\ \text{pN/s}} = 10^{-5}$. In this range of loading rates, Fig. 2 shows that $\tilde{f}^*$ varies almost linearly with $\ln \tilde{r}$ for the harmonic model.

At higher loading rates, the force spectrum is not linear anymore. However, these values of loading rates are much too high to be experimentally accessible and correspond to applied forces close to the critical one, meaning that Kramer's theory [Eqs. (1)–(5)] is not valid anymore. Hence these high loading rates are of little interest for the experimentalist. For recent developments concerning the force spectroscopy of a single bond close to the critical force and the predicted nonlinearity of the force spectrum, see Refs. [38–40]. Thus both models lead in practice to a linear force spectrum and cannot be distinguished by studying only the force spectrum.

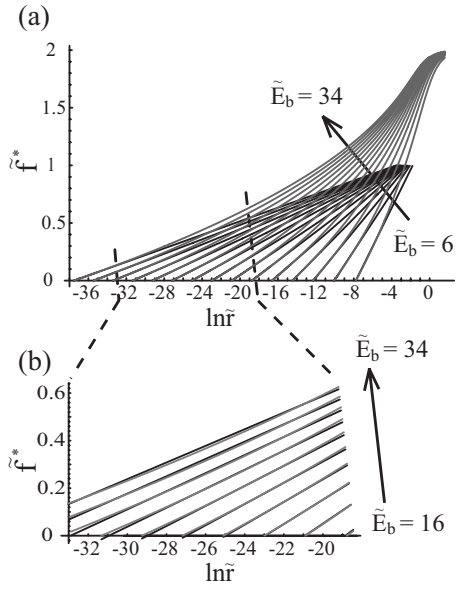

FIG. 2. Plots of $\tilde{f}^*$ vs $\ln \tilde{r}$ obtained with the Bell model and the harmonic model, for different values of $\tilde{E}_b$. (a) For very wide variation of $\ln \tilde{r}$, the force spectra are nonlinear with the harmonic model (gray lines) whereas they are straight lines with the Bell model (black lines). $\tilde{E}_b$ varies from 6 to 34, with a increase of 2 between successive spectra. The dotted lines limit the experimentally accessible region. (b) In this experimentally accessible region, the harmonic model gives almost linear spectra (gray lines), which are superimposed with linear fits (gray lines).$\tilde{E}_b$ varies from 16 to 34, with a increase of 2 between successive spectra.

It is worth noting that this result means that, contrarily to the common belief, a linear force spectrum is not evidence of the validity of the Bell model.

In order to estimate the error made by using the inappropriate shape of the landscape, a linear approximation of the force spectrum given by the harmonic model [Eq. (17)] over the experimentally relevant loading rates can be computed for each value of $\tilde{E}_b$. This approximation leads to

$$\tilde{f}^* = P_1(\tilde{E}_b)\frac{\ln \tilde{r}}{\tilde{E}_b} + P_2(\tilde{E}_b)\left(1 + \frac{\ln \tilde{E}_b}{\tilde{E}_b}\right), \tag{18}$$

where $P_1(\tilde{E}_b)$ and $P_2(\tilde{E}_b)$ constrained to be linear functions of $\tilde{E}_b$: $P_1(\tilde{E}_b) \approx 7.92 \times 10^{-1} + 1.17 \times 10^{-2}\tilde{E}_b$ and $P_2(\tilde{E}_b) \approx 8.20 \times 10^{-1} + 1.02 \times 10^{-2}\tilde{E}_b$ were obtained numerically. The resulting slope and intercept (functions of $\tilde{E}_b$), were then approximated by the *a priori* form $\frac{P_1(\tilde{E}_b)}{\tilde{E}_b}$ and $P_2(\tilde{E}_b)\left(1+\frac{\ln \tilde{E}_b}{\tilde{E}_b}\right)$, respectively. We note that, strictly speaking, $P_1(\tilde{E}_b)$ and $P_2(\tilde{E}_b)$ also depend on x_b and t_D because the experimentally accessible range—over which the fit with Eq. (17) is evaluated—does.

As a result, although actually linear, the force spectrum given by the harmonic model has a different slope and intercept with the $\ln \tilde{r}=0$ axis. For a given common value of $\frac{E_b}{x_b}$, and hence a comparable value of $\tilde{f}^*$ in the nondimensional equations (15) and (17), the relative difference between the slope and the intercept of the force spectrum given by both models is a function of $\tilde{E}_b$: it is directly given by the functions $P_1(\tilde{E}_b)$ and $P_2(\tilde{E}_b)$, which reach up to 15–20% for high barriers (e.g., $\geqslant 30k_BT$), $x_b=0.31$ nm and $t_D=2.1\times10^{-11}$ s. Conversely, for a given t_D, one can also determine different energy landscapes referring to each model. This view is important for the experimentalist who wants to fit a (dimensional) force spectrum $f^*(\ln r)$, and who will obtain model dependant energy landscapes. To obtain the parameters (E_b^{Bell}, x_b^{Bell}) and (E_b^{harm}, x_b^{harm}) corresponding to the energy landscape given by the Bell and the harmonic models, respectively, one can equate

$$f^* = \frac{E_b^{Bell}}{x_b^{Bell}}\left[\frac{1}{\tilde{E}_b^{Bell}}\ln\frac{r}{\frac{E_b^{Bell}}{x_b^{Bell}t_D}} + \left(1+\frac{\ln \tilde{E}_b^{Bell}}{\tilde{E}_b^{Bell}}\right)\right]$$

and

$$f^* = \frac{E_b^{harm}}{x_b^{harm}}\left[\frac{P_1(\tilde{E}_b^{harm})}{\tilde{E}_b^{harm}}\ln\frac{r}{\frac{E_b^{harm}}{x_b^{harm}t_D}} + P_2(\tilde{E}_b^{harm})\left(1+\frac{\ln \tilde{E}_b^{harm}}{\tilde{E}_b^{harm}}\right)\right].$$

This leads to

$\tilde{x}_b^{harm}/\tilde{x}_b^{Bell} = P_1(\tilde{E}_b^{harm})$ and

$$\frac{E_b^{harm}}{E_b^{Bell}} = \frac{P_1(\tilde{E}_b^{harm})/P_2(\tilde{E}_b^{harm})}{1+[1-P_1(\tilde{E}_b^{harm})/P_2(\tilde{E}_b^{harm})](\ln \tilde{E}_b^{harm}/\tilde{E}_b^{harm}) + [P_1(\tilde{E}_b^{harm})/P_2(\tilde{E}_b^{harm})][\ln P_1(\tilde{E}_b^{harm})/\ \tilde{E}_b^{harm})]},$$

hence the relative errors $\frac{x_b^{harm}-x_b^{Bell}}{x_b^{Bell}}$ and $\frac{E_b^{harm}-E_b^{Bell}}{E_b^{Bell}}$. Figure 3 shows a plot of these relative errors, for two sets of values ($x_b=0.31$ nm; $t_D=2.1\times10^{-11}$ s) and ($x_b=0.5$ nm;

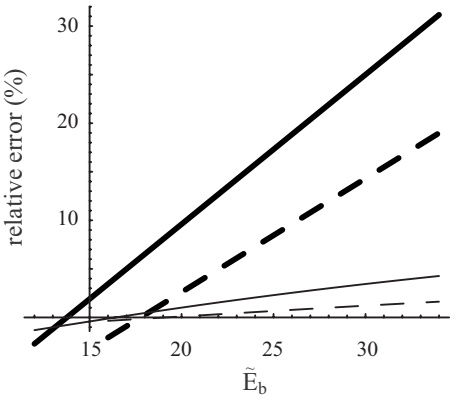

FIG. 3. Plot of $\frac{x_b^{harm}-x_b^{Bell}}{x_b^{Bell}}$ and $\frac{E_b^{harm}-E_b^{Bell}}{E_b^{Bell}}$ vs $\tilde{E}_b=\frac{E_b^{harm}}{k_BT}$. In a first example (corresponding to the streptavidin-biotin bond) with $x_b^{harm}=0.31$ nm and $t_D=2.1\times10^{-11}$ s, $\frac{x_b^{harm}-x_b^{Bell}}{x_b^{Bell}}$ is in a thick dashed line and $\frac{E_b^{harm}-E_b^{Bell}}{E_b^{Bell}}$ is in a thin dashed line. In a second example with $x_b^{harm}=0.5$ nm and $t_D=10^{-9}$ s, $\frac{x_b^{harm}-x_b^{Bell}}{x_b^{Bell}}$ is in a thick solid line and $\frac{E_b^{harm}-E_b^{Bell}}{E_b^{Bell}}$ in a thin solid line.

$t_D=10^{-9}$ s). As shown in Fig. 3, these relative errors become on the order of 30% for high energy barriers ($\geqslant 30k_BT$). Thus if such errors are acceptable for the experimentalist, the Bell model will provide a sufficiently good approximation of the landscape. Therefore the Bell model can be used to analyze experiments on bonds whose landscapes are harmonic and vice versa, the harmonic model can be used to analyze bonds whose landscape is fully described by the Bell model. If a better description of the landscape is required, one may hope that a detailed study of the whole set of rupture-force distributions may help differentiating the two models.

G. Rupture force distributions and influence of the experimental error

An example of rupture-force distribution $p(f)$ obtained with the harmonic model for several loading rates is given in Fig. 4(a) (solid line). These distributions are experimentally relevant since they are obtained with the parameters that we extracted from the analysis of our experimental data on the streptavidin-biotin bond (namely $x_b=0.31$ nm, $Eb=32k_BT$, and $t_D=2.1\times10^{-11}$ s; see Ref. [8] for details). For comparison, the distributions that would be obtained with the Bell approach are also given in Fig. 4(a) (dotted line). With both models, energy landscapes with the same parameters (i.e., the same x_b, E_b, and t_D) do not give exactly the same distributions. Thus the set of experimental distributions may indicate the shape of the energy landscape that has to be used for the analysis. The previous discussion shows that linear force spectra are always predicted. Thus f^* will not allow differentiating between the models. In addition to f^*, a few relevant parameters are sufficient to describe the main features of the distributions: the maximum of the distribution, $p(f^*)$, the average force $\langle f\rangle$, and the width of the force distribution w. The expressions of these parameters are given in Appendix A. As an example, Fig. 5 shows a plot of f^* and $\langle f\rangle$,

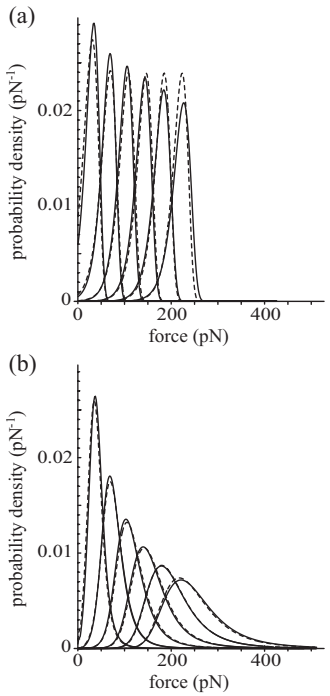

FIG. 4. Plot of rupture force distributions $p(f)$ vs the applied force f, for $x_b=0.31$ nm, $E_b=32k_BT$, and $t_D=2.1\times10^{-11}$ s. (a) $p(f)$ obtained with the Bell model (dashed curves) and with the harmonic model (solid curves). The loading rate varies from 0.1 to $\sim3\times10^4$ pN/s. (b) Effective distributions $p^{eff}(f)$ obtained from the theoretical distributions $p(f)$ by taking into account the experimental error modelized as Gaussian of width $\sigma(f)$ (see text for details). The same values for x_b and E_b were used in the harmonic model to calculate $p^{eff}(f)$, whereas new values x_b^{Bell} and E_b^{Bell} where calculated following the procedure explained in Sec. II F so that the most probable rupture force f^* obtained by both models would match. The effective distributions $p^{eff}(f)$ were obtained from these $p(f)$ with coinciding f^* (dashed curves for the Bell model, solid curves for the harmonic model), and it appears clearly that after taking into account the experimental error, no difference can be observed between the rupture force distributions given by both models.

while Fig. 6 shows a plot of w and $p(f^*)$—for both models and in the case of the streptavidin-biotin bond. As expected from Sec. II F, f^* does not significantly differ between the two models. In contrast, the variations of $\langle f\rangle$ and $p(f^*)$ with $\ln r$ seem sufficiently different in order to discriminate between the two models. However, these theoretical considerations do not correspond to the experimental reality where errors always exist.

The experimental error can be included in the analysis by changing a given rupture force probability density $p(f)$ to an effective rupture force probability density $p_{eff}(f)$ by using the relationship

$$p_{eff}(f)=\int_0^{+\infty}p(\alpha)\exp\left(-\frac{(\alpha-f)^2}{2\sigma(f)^2}\right)d\alpha, \qquad (19)$$

where the Gaussian error has a width $\sigma(f)$, which is inspired by the experiments. Briefly, in a quite general case the ex-

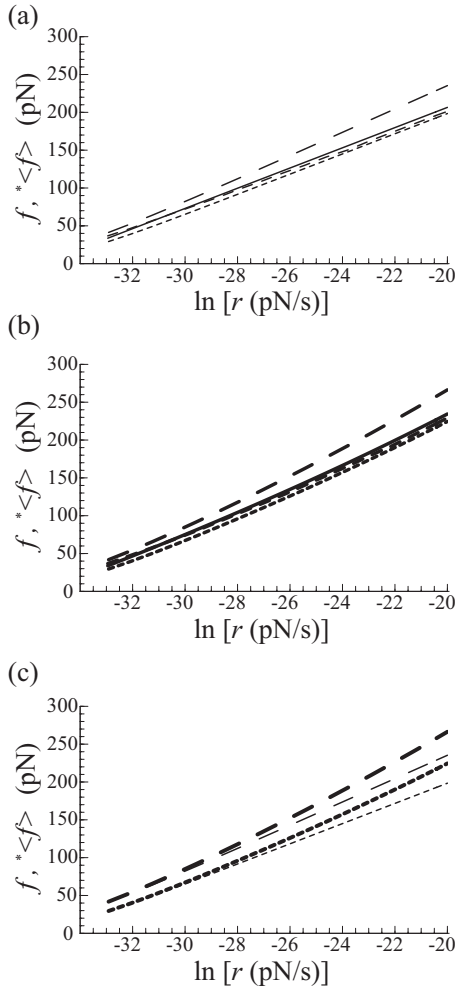

FIG. 5. Average and most probable rupture forces obtained with the Bell model and the harmonic model, for $x_b=0.31$ nm, $E_b=32k_BT$, and $t_D=2.1\times10^{-11}$ s. (a) The Bell model. The most probable rupture force f^*, before (thin solid line) and after (thin medium-dashed line) taking experimental error into account [i.e., maxima of $p(f)$ and $p^{eff}(f)$, respectively] are very close, while the averaged force $\langle f\rangle$ before (thin short-dashed line) and after (thin large-dashed line) taking the experimental error into account show a marked difference. (b) Similar conclusion for the harmonic model. Most probable rupture force before f^* before (thick solid line) and after (thick medium-dashed line) taking experimental error into account; averaged force $\langle f\rangle$ before (short-dashed thin line) and after (thick large-dashed line) taking the experimental error into account (large-dashed thin line) show a marked difference. (c) Superposition of the most probable and average rupture force before and after taking the experimental error into account for both models [same line symbols as in (a) and (b)].

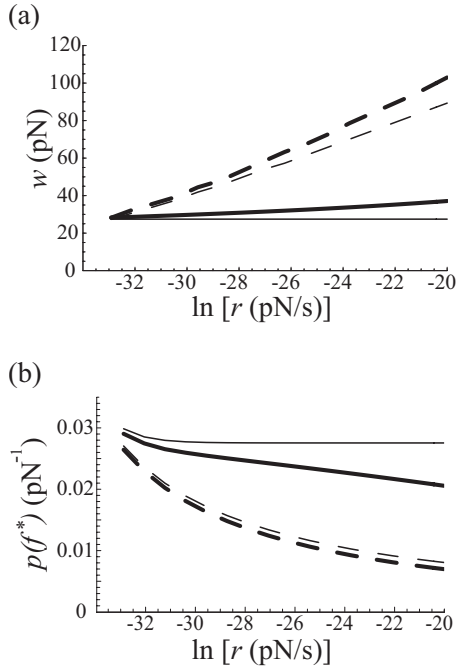

FIG. 6. Plot of the width w of the rupture force distributions and maximum probability density $p(f^*)$ vs $\ln r$ for the Bell model and the harmonic model. The parameters $x_b=0.31$ nm, $E_b=32k_BT$, and $t_D=2.1\times10^{-11}$ s are used in both models. (a) w before (thin solid line for the Bell model, thick solid line for the harmonic model) and after (thin dashed line for the Bell model, thick dashed line for the harmonic model) taking the experimental error into account. Clearly, by taking it into account, the width of the distribution greatly increases for both models. (b) $p(f^*)$ before (thin solid line for the Bell model, thick solid line for the harmonic model) and after (thin dashed line for the Bell model, thick dashed line for the harmonic model) taking the experimental error into account.

erted force f is equal to kx, where k is the spring constant and x the spring extension. Therefore $df=kdx+xdk=kdx+f\frac{dk}{k}$. dx is a constant due to the thermal fluctuations and the accuracy on the detection of the position of the bead in a single-molecule experiment. In our case [8], we performed experiments with a biomembrane force probe, and thus kdx is of the order of 100 pN/μm$\times$10 nm=1 pN. The error on k, in the case of a biomembrane force probe, is mainly due to the poor accuracy on various length measurements (inner diameter of the pipette, diameter of the red blood cell, and diameter of the contact between the red cell and the bead, all of the order of 1 μm); this error can be estimated to be between 10 and 30%. Following these constraints, we chose $\sigma(f)=\mathrm{Max}[1,0.2f]$ (in pN). Using this expression for $\sigma(f)$, we computed the effective experimental distributions $p^{eff}(f)$ [Fig. 2(b)]. Once shifted in order to compare distributions with a common f^*, $p_{eff}(f)$ given by both models almost perfectly overlap [Fig. 4(b)]. The corresponding values for f^*, $\langle f\rangle$, and $p(f^*)$ are given in Figs. 5 and 6. Thus the experimental error does not change the force spectrum but erases the differences between the two models for $\langle f\rangle$, $p(f^*)$, and w^*. As a result, neither the average force nor the width of the distribution or the value at its maximum can be easily used to deduce the shape of the energy landscape from experimental rupture forces.

To summarize this part, we have shown that experimental errors make it difficult to derive information on the energy landscape from the force distribution. Experimentally, the limited amount of data points that will be available makes it even more complicated. The influence of the experimental error on the shape of the distribution has also been discussed elsewhere with a different approach [41]. Hence, ultimately,

only the most likely force, i.e., the force spectrum, is relevant for the analysis of experiments. This shows that it is not possible to deduce the exact shape of the landscape from the whole set of rupture-force distributions. In this situation, where the exact shape is unknown, t_D is also unknown. Then, Eqs. (2) and (11) indicate that, in both the Bell and harmonic models, t_D and E_b are coupled and that it will therefore be impossible to uncouple them. Therefore the height and position of the barrier are the only features of the energy landscape that can be found, provided that t_D can be well-estimated. Finally, our study shows that the Bell and harmonic models cannot be distinguished. Since the Bell model is simpler, it is usually more appropriate to use it.

III. PIECEWISE-LINEAR ENERGY LANDSCAPE MODEL

The harmonic model does not have more predictive power than the Bell model. The latter being simpler to handle, it is reasonable to use it to analyze experiments with single energy barriers. In Sec. II, we concluded that the use of the Bell model to analyze force rupture measurements would lead to a landscape within a 30% error of any landscape presented in Fig. 1. However, in this family of landscapes, the tangential connection leading to Eq. (10) limits the extent of landscapes taken into account. Energy landscapes with "steep slopes," i.e., with a critical force larger than $2E_b/x_b$, are not included in this family. In this section we numerically solve the time evolution equation with piecewise-linear energy landscapes in order to significantly widen the studied shapes.

A. Model

Let us consider a reaction coordinate x which is divided into N segments $[x_i,x_{i+1}]$ with $i=0\cdots N-1$ of equal length. Over each of these N segments, the energy landscape is supposed to be a linear nondecreasing function of x. At each x_i, the energy is constrained to take a value $E_i \in \{\frac{i}{N}E_b, i=0\cdots N-1\}$. Furthermore, the energy landscape is imposed to be continuous, with the additional constraints $E(x=0)=0$ and $E(x=x_b)=E_b$. In this piecewise-linear model, the zero-force situation is always one with a single energy barrier located at $x=x_b$ with an energy minimum located at $x=0$. This model is a generalization of the Bell model since the particular case $N=1$ exactly leads to Bell's results. For simplicity we consider a common value of t_D over the whole reaction coordinate. As we previously noted, following Eq. (2) a change of t_D is equivalent to a translation on the energy scale. For the calculation of the off-rate $k_{off}(f)$ at a given force f, the Bell model is applied to the barrier with the actual minimum location for this force f. For each N, there are $\frac{1}{2}\binom{2N}{N}$ associated energy landscapes. As an example, the ten landscapes corresponding to $N=3$ are displayed in Fig. 7. Because the time evolution equation was numerically solved in this case, we chose to focus on the force spectrum and we did not investigate any other parameter such as the average rupture force or the distribution width, which strongly depend on the experimental error (see Sec. II). The solution of the time evolution equation was obtained with MATHEMATICA (the corresponding program is available upon request).

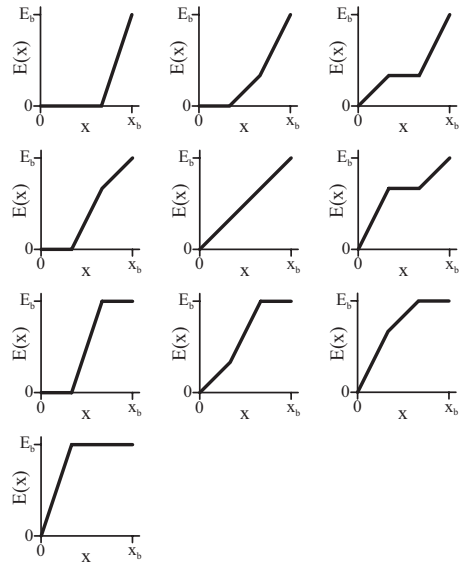

FIG. 7. Plots of the ten piecewise-linear energy landscapes treated by the model described in Sec. III for $N=3$.

B. Consequences of the shift of the position of the minimum and maximum of the energy landscape

One main difference between the harmonic and the Bell model is that in the first one, the barrier location on the reaction coordinate axis evolves with the increasing applied force. In the piecewise-linear model, as soon as $N\geqslant 2$, the minimum and maximum's location on the reaction coordinate axis can vary as well as a function of force. The latter situation can arise where the minimum location shifts from $x=0$ to a new value $x=x_m>0$ when the applied force reaches a threshold value. In an equivalent manner the position of the energy maximum may shift from $x=x_b$ to $x=x_{b2}<x_b$. Figure 8(a) shows an example with $N=5$ and $E_b=32k_BT$, where the position of the minimum shifts from $x=0$ to $x_m=\frac{4}{5}x_b$ as soon as $f>0$. The resulting force spectrum has a slope which is $\frac{k_BT}{x_b-x_m}$ which in this example is five times higher than the slope $\frac{k_BT}{x_b-0}$ of the force spectrum that is obtained when applying the Bell model to the energy landscape.

We are now tackling a profound difficulty that could already be suspected from the study of the two models in Sec. II: differences in slopes as high as an order of magnitude can be found from one energy landscape to another with the same height and position of the barrier. That is to say that the prediction obtained with the Bell model (or any other model such as the harmonic model) is significantly inaccurate in that case. In the example given in Fig. 8(a), the Bell model would predict a value for x_b five times smaller than the actual one. Similarly, the harmonic model would predict wrong parameters with a similar error.

C. Single energy barrier giving rise to multiple barriers under force: Varying slopes, plateaus, and linearity of the force spectrum

Regarding the force spectrum, the piecewise-linear model predicts even richer features than a different slope from the

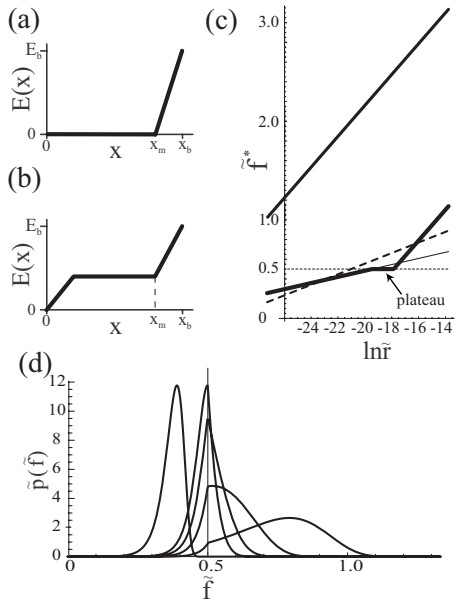

FIG. 8. (a) Energy landscape obtained with $N=5$ in the model described in Sec. III. The position of the energy minimum shifts from $x=0$ to $x_m=\frac{4}{5}x_b$ as soon as the applied force $f>0$. (b) Other piecewise-linear energy landscape obtained with $N=5$, for which position of the energy minimum shifts from $x=0$ to $x_m=\frac{4}{5}x_b$ as soon as the applied force f is higher than a nonzero threshold f_s (in this particular case $f_s=\frac{1}{2}\frac{E_b}{x_b}$). $\tilde{E}_b$ is set equal to 32. (c) The force spectrum obtained with the energy landscape plotted in (a) is plotted in a medium-thickness solid line. As the position of the minimum shifts as soon as $f>0$, the force spectrum has a slope much higher than the one that would have been predicted by the Bell model (in a thin solid line). The force spectrum obtained with the energy landscape plotted in (b) is plotted in a thick solid line. It exhibits two different linear regimes when the loading rate increases, and a plateau between these two regimes. The dashed line represents a linear fit to this force spectrum. (d) Rupture force distributions corresponding to the energy landscape plotted in (b). The force $\tilde{f}=\frac{1}{2}$ at which the shift of the energy minimum occurs is shown by a vertical line.

Bell model. As we saw previously, in some cases the shape of $E(x)$ is such that the energy-minimum position or the energy-maximum position (or both) shifts from $x=0$ to a new value $x=x_m$ (or from $x=x_b$ to a new value $x=x_{b2}$) after a certain force level is reached. In these cases the single barrier, by performing the shift under force, behaves as if two different energy barriers of a complex energy landscape were successively probed under force. The study of complex bonds [14,15,24,42] exhibiting different main energy barriers has been introduced and studied in depth by Evans *et al.* since the 1990s; and as explained by the authors in Ref. [14], the signature of the dynamic force spectroscopy of such a complex bond is a force spectrum exhibiting several linear regimes, with increasing slopes.

What we observe here with the piecewise-linear model describing a single-barrier energy landscape is very similar: the force spectrum exhibits different linear regimes when the loading rate increases [see Fig. 8(c)]. But this model follows a new and striking behavior: in between two linear regimes, the force spectrum can exhibit a plateau of the most likely rupture force. Such a behavior can be explained when looking at the probability distribution of rupture force $p(f)$. Indeed, if we name the force at which the shift of one energy extremum happens f_s, then the distribution $p(f)$ can be written as

$$p(f)=p_1(f) \quad \text{if } f \leqslant f_s,$$

$$p(f)=p_2(f) \quad \text{if } f \geqslant f_s, \tag{20}$$

where $p_1(f)$ is the distribution given by the Bell model applied to the barrier before the shift, whereas $p_2(f)$ is the distribution given by the Bell model applied to the barrier after the shift [see Fig. 8(d)].

Thus a bond described by a single-barrier energy landscape can lead to a force spectrum with various linear regimes and with a plateau in between them. The fraction of landscapes exhibiting such behavior is not negligible (a few tens of percent). However, the width of the plateau in all the studied landscapes never covered more than one order of magnitude for the loading rate, making it very difficult, if not impossible, to be experimentally observed. Similarly, in most cases, the presence of the plateau makes it unlikely for the two linear regimes to be experimentally observed. In the majority of the cases, the force spectrum will appear to be a single regime with a slope in between the ones of the two regimes.

In conclusion, even though the predicted force spectrum can display very unusual features, it will almost always experimentally seem to be linear. Thus the slope and the intercept with the y axis fully define the corresponding force spectrum.

D. Average over all landscapes and universal relation between E_b, x_b, and the force spectrum

In this paragraph, we used the normalized variables in order to obtain the distributions for all the landscapes corresponding to E_b ranging from $5k_BT$ to $40k_BT$. For a computer-time consuming reason we chose not to go further than $N=8$, which gives already a good approximation of any energy landscape with x_b smaller than a few nm (accuracy of $\pm 0.06\times x_b$ in distance and $\pm \mathrm{E_b}/16$ in energy). We also limited the loading rates to realistic experimental values (between 0.1 pN/s and 0.1 μN/s for $x_b=1$ nm) for $E_b>15k_BT$. For smaller values of E_b, loading rates between 0.1 μN/s and 10 mN/s had to be taken in order to obtain a nonzero most likely rupture force f^*. As mentioned in the previous paragraph, only two parameters are required in order to describe the experimentally linear force spectrum: the slope, $\tilde{s}$, and the intercept with the y axis, $\tilde{f}_0$. For the Bell model, $\tilde{s}=\frac{1}{\tilde{E}_b}$ and $\tilde{f}_0=1+\frac{\ln \tilde{E}_b}{\tilde{E}_b}$.

For a given energy, we considered all the landscapes obtained with N ranging from 2 to 8 (i.e., a total of 8787 landscapes per energy value). Then for each energy value, we plot $\tilde{f}_0$ vs $\tilde{s}$, i.e., 8787 points of coordinates $(\tilde{s},\tilde{f}_0)$. Figure 9 shows the cases $E_b=15k_BT$, $20k_BT$ and $32k_BT$. The expected values for the Bell and harmonic models (i.e., two particular

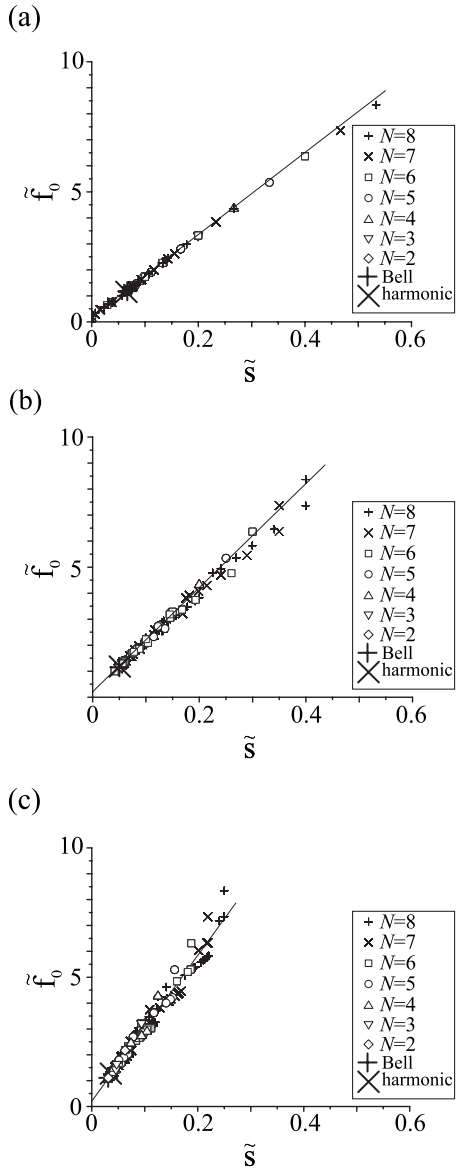

FIG. 9. Plots of the intercept $\tilde{f}_0$ of force spectra with the $\ln \tilde{r}=0$ vs their slope $\tilde{s}$. For three different energy values, all the landscapes obtained with N ranging from 2 to 8 were considered, as well as the landscapes treated by the Bell model and the harmonic model. The different figures correspond to different values of E_b. At a given energy, the solid line is a linear fit to the points. (a) $E_b=15k_BT$, (b) $E_b=20k_BT$, and (c) $E_b=32k_BT$.

points) are also inserted on the graphs. In good approximation, all the $(\tilde{s},\tilde{f}_0)$ points coming from the various landscapes belong to a single line. This could be expected for some landscapes in which the minimum and the maximum continuously shift and will display a force spectrum following the Bell model with a smaller x_b. However, this was not easy to predict for most landscapes, including those with a plateau in their force spectrum. This linear behavior was observed for all studied E_b values. The plot of $\tilde{f}_0$ vs $\tilde{s}$ has a slope that we note σ_1, and an intercept with the y axis that we note σ_2, which are *a priori* functions of E_b. They are given in Fig. 10. σ_2 is almost constant and equal to 0.21. Below $40k_BT$, a good

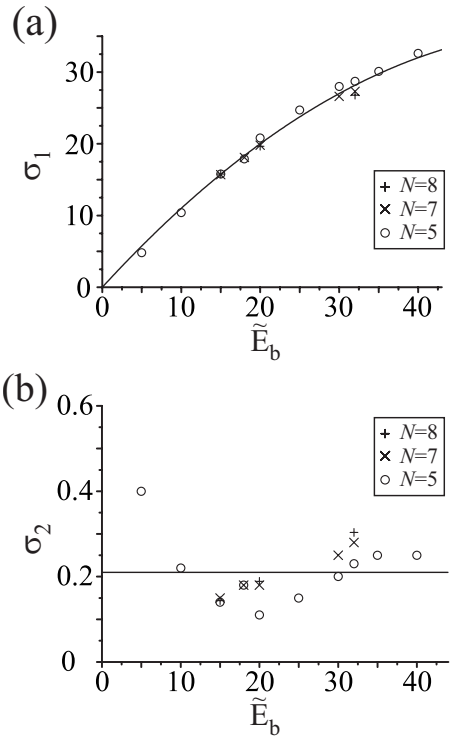

FIG. 10. (a) Plot of σ_1 vs $\tilde{E}_b$ obtained for $N=5$, 7, and 8. The solid line is a parabolic fit to these points: $\sigma_1 \approx -0.01\tilde{E}_b+1.2\tilde{E}_b$. (b) Plot of σ_2 vs $\tilde{E}_b$ obtained for $N=5$, 7, and 8. By fitting σ_2 with a constant value (solid line), one gets $\sigma_2 \approx 0.21$.

approximation of σ_1 is given by $\sigma_1=-0.01\tilde{E}_b^2+1.2\tilde{E}_b$. An approximated relation between $\tilde{s}$ and $\tilde{f}_0$ can then be obtained:

$$\tilde{f}_0=(-0.01\tilde{E}_b^2+1.2\tilde{E}_b)\tilde{s}+0.21. \tag{21}$$

Thus for the nondimensional variables, a given set $(\tilde{s},\tilde{f}_0)$ is sufficient to obtain $\tilde{E}_b$. The subsequent average and standard deviation of $\tilde{E}_b$ are given in Table I [the values $(\tilde{s},\tilde{f}_0)$ ob-

TABLE I. Each value of $\tilde{E}_b$ from the first column was injected in Eq. (21), then the set of values $(\tilde{s},\tilde{f}_0)$ obtained for each piecewise-linear energy landscape with $N \leqslant 8$ gave the average value extracted from Eq. (21) for $\tilde{E}_b$ (second column), and its spread (third column). By injecting the two particular couples $(\tilde{s},\tilde{f}_0)$ corresponding to the Bell model and the harmonic model at $\tilde{E}_b$ equal to the value in the first column, we obtained the value predicted by Eq. (21) (fourth and fifth column, respectively).

E_b (units of k_BT)	$\langle E_b \rangle$ (units of k_BT)	σ_{E_b} (units of k_BT)	E_b^{Bell} (units of k_BT)	E_b^{harm} (units of k_BT)
20	19.1	0.6	18.5	19.3
25	24.6	1.1	23.9	26.8
32	33.0	2.8	33.6	34.4

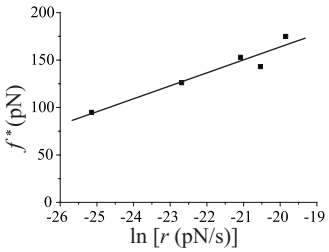

FIG. 11. Force spectrum measured for deepest minimum of the streptavidin-biotin energy landscape [8]. The solid line is a linear fit to the data.

tained for each landscape were injected in Eq. (21) and a corresponding value of $\tilde{E}_b$ was calculated].

The remaining problem is that a prerequisite to derive dimensionless data is to know x_b, before even performing the measurements. If this is not the case, only a "universal" relation between x_b, E_b, and the force spectrum can be obtained by switching back to physically measurable variables:

$$s \ln\left(\frac{E_b}{x_b t_D r_0}\right) + f_0 = \left[-0.01\left(\frac{E_b}{k_B T}\right)^2 + 1.2\frac{E_b}{k_B T}\right] s + 0.21\frac{E_b}{x_b}, \tag{22}$$

where r_0 is such that the y axis is defined by $\ln r = \ln r_0$ (with r_0 a fixed arbitrary value, 1 pN/s for instance). Note that f_0 is the intercept with the y axis obtained directly from the experimental plot of f^* vs $\ln r$. Then f_0 is not simply equal to $\frac{E_b}{x_b}\tilde{f}_0$ but to $\frac{E_b}{x_b}\tilde{f}_0 + s \ln\left(\frac{r_0}{E_b/x_b t_D}\right)$. Table I shows that Eq. (22) is valid with a good approximation for any shape of the energy landscape. In the next section we will show how it can be applied to actual experimental measurements.

IV. EXPERIMENTAL DATA ANALYZED BY DIFFERENT MODELS

We applied both the Bell and the harmonic models to the streptavidin-biotin interaction. Our previous work on this ligand-receptor-type interaction [8] showed that the energy landscape of the bond is complex in the sense that it exhibits three main energy barriers. However, when pulling the bond once it had sufficient time to relax to the deepest energy minimum, the energy landscape of the bond can be modeled as having a single energy barrier (x_b=0.31 nm, $E_b=32k_BT$), because the other intermediate barriers are never expected to be the highest at any force. As expected in these experimental conditions, the force spectrum, displayed in Fig. 11, is linear. We applied both models to fit the linear force spectrum, and then extracted the resulting parameters for the main energy barrier dominating the kinetics of the bond under these initial conditions, and for this loading rate range. With the Bell model, we obtained the values x_b=0.30 nm and $E_b=30.7k_BT$, with a value for the microscopic time which we set equal to the one used in the harmonic model, i.e., $t_D=2.1\times10^{-11}$ s. With the harmonic model, we had additional constraints over the energy landscape curvatures in order to fit experimental data [8], and they led to a value of $t_D=2.1\times10^{-11}$ s, x_b=0.31 nm, and $E_b=32k_BT$. Fitting the force spectrum while relaxing the constraints on E_b taken into account in Ref. [8] leads to $E_b=31.1k_BT$. The error over E_b and x_b is thus of only a few percents: as expected from the results in Sec. II, the Bell model and the harmonic model are in close agreement, provided that a common t_D is taken.

We used Eq. (22) by injecting the values s=13.6 pN and f_0=437 pN (with a y axis defined by $r_0=1N/s$) obtained by fitting the experimental force spectrum. In addition, we injected in the relation the value of x_b obtained with the Bell model and the harmonic model, respectively. The "universal" relation gives the value $E_b=32.3k_BT$ with x_b=0.30 nm derived from the Bell model (thus a 5% error), and $E_b=29.3k_BT$ with x_b=0.31 nm derived from the harmonic model (thus a 6% error). Both energy values obtained by injecting the value of x_b in Eq. (22) are thus very close to the value obtained by each respective model. Now by inserting the energy values obtained by both models into Eq. (22), one can obtain in return values for x_b. Inserting $E_b=30.7k_BT$ obtained with the Bell model gives x_b=0.25 nm; by inserting $E_b=31.1k_BT$ and $E_b=32k_BT$ obtained with the harmonic model depending on the additional constraints, one gets x_b=0.26 and 0.29 nm, respectively (i.e., a 16% and 6% error, respectively).

In this example of the streptavidin-biotin bond, the Bell model and the harmonic model predict values for x_b and E_b in close agreement. In Appendix B, we give another example—but in this case of experiments performed under constant applied force—where both models are in close agreement. We point out that if both models are in close agreement here, this does not mean that the values for x_b and E_b are correct: there could be, for instance, as explained in Sec. III, a shift in the energy minimum position during the pulling process, leading to a x_b much shorter than the real one. But in this particular study of the streptavidin-biotin bond, supplementary studies provided us with constraints excluding these particular cases [8].

V. CONCLUSION

The analyses of the Bell and harmonic models have shown that the Bell approximation is acceptable in most cases. Usually, it leads to parameters x_b and E_b from single-molecule rupture forces in close agreement with the ones predicted by the harmonic model, which encompasses a broader class of energy landscape shapes. Nevertheless, if no supplementary information is available about the studied bond, a value for t_D has to be postulated, otherwise the absolute value of E_b is not known.

By taking the experimental error into account, we showed that force spectrum of a single bond, i.e., f^* vs $\ln r$, is the most important input for the analysis of experimental data. An analysis based on other variables like the average rupture force, the width, or maximum value of the rupture-force distribution is risky because they are highly dependent on experimental error, whose precise form is very difficult to measure independently.

Our study of a piecewise-linear energy landscape showed that there are some cases for which the Bell model and the

harmonic model break down simultaneously, with unacceptable error levels. These cases form a class of energy landscape shapes where essentially the current analysis of single-molecule rupture forces loses any predictive power. However, we showed that, whatever its shape, a single barrier can be partly described by applying a universal law to the force spectrum. This analysis provides a relation between the force spectrum and parameters x_b and E_b, the latter depending on the value of t_D. Any complementary information, be it experimentally or from computer simulations, providing one of the parameters x_b or E_b, is sufficient to determine the remaining one through the universal relation.

This study was restricted to single-barrier energy landscapes, but it already exhibited a great variety of features and there is still some progress to make in the analysis of these "simple" landscapes. Complex energy landscapes with more than one energy barrier, or even more than one reaction pathway are already included in recent models and will certainly prove to be even richer in surprising and unusual features. They have to be carefully studied in the near future.

ACKNOWLEDGMENTS

The authors are grateful to P. Charbonneau and E. Perez for reading the manuscript.

APPENDIX A: EXPRESSIONS OF w, $\langle\tilde{f}\rangle$, AND $p(f^*)$ FOR THE BELL AND THE HARMONIC MODELS

1. Width of the rupture force distribution, w^*

For the Bell model and the harmonic model, the integral in Eq. (5) can be handled and has an analytical result. With the Bell model, one gets

$$\tilde{p}(\tilde{f}) = \frac{1}{\tilde{r}} \exp\left(\tilde{E}_b(\tilde{f}-1) + \frac{e^{-\tilde{E}_b}}{\tilde{r}\tilde{E}_b}(1-e^{\tilde{f}\tilde{E}_b}) \right), \tag{A1}$$

which is useful to put under the form

$$\tilde{p}(\tilde{f}) = \tilde{p}(\tilde{f}^*)\exp[\tilde{E}_b(\tilde{f}-\tilde{f}^*) - e^{(\tilde{f}-\tilde{f}^*)\tilde{E}_b} + 1], \tag{A2}$$

whereas with the harmonic model:

$$\tilde{p}(\tilde{f}) = \exp\left(\frac{1}{\tilde{r}}\sqrt{\frac{\pi}{\tilde{E}_b}} \left\{ \mathrm{erf}\left[\sqrt{\tilde{E}_b}\left(1-\frac{\tilde{f}}{2}\right)\right] - \mathrm{erf}(\sqrt{\tilde{E}_b}) \right\} \right), \tag{A3}$$

which likewise can be written under a more suitable form:

$$\begin{aligned}\tilde{p}(\tilde{f}) = \tilde{p}(\tilde{f}^*)\exp\Bigg(& \tilde{E}_b\left(1-\frac{\tilde{f}^*}{2}\right)^2 - \tilde{E}_b\left(1-\frac{\tilde{f}}{2}\right)^2 \\ & + \frac{1}{\tilde{r}}\sqrt{\frac{\pi}{\tilde{E}_b}}\left\{ \mathrm{erf}\left[\sqrt{\tilde{E}_b}\left(1-\frac{\tilde{f}}{2}\right)\right] \right. \\ & \left. - \mathrm{erf}\left[\sqrt{\tilde{E}_b}\left(1-\frac{\tilde{f}^*}{2}\right)\right] \right\} \Bigg).\end{aligned} \tag{A4}$$

Both models give distributions that exhibit the following features.

(i) Below a certain minimal (nondimensional) loading rate $\tilde{r}_m = \frac{\exp(-\tilde{E}_b)}{\tilde{E}_b}$, $\tilde{f}^* = 0$, that is to say that $\tilde{p}(\tilde{f})$ is a decreasing function of $\tilde{f}$.

(ii) Above the minimal loading rate $\tilde{r}_m$, $\tilde{p}(\tilde{f})$ is a bell-shaped distribution, whose width can be determined from Eqs. (20) and (22). In the region $\tilde{r} > \tilde{r}_m$, for a sufficiently high loading rate, the equation $\frac{\tilde{p}(\tilde{f})}{\tilde{p}(\tilde{f}^*)} = e^{-1/2}$ has two positive solutions, whose difference gives the width of the distribution. One finds for the Bell model $\tilde{w} \approx \frac{1.028}{\tilde{E}_b}$, whereas for the harmonic model, one can derive from Eq. (22), expanding $\mathrm{erf}\left[\sqrt{\tilde{E}_b}\left(1-\frac{\tilde{f}}{2}\right)\right]$ in the vicinity of $\mathrm{erf}\left[\sqrt{\tilde{E}_b}\left(1-\frac{\tilde{f}^*}{2}\right)\right]$ as a function of $\varepsilon = \mathrm{erf}\left[\sqrt{\tilde{E}_b}\left(\frac{\tilde{f}-\tilde{f}^*}{2}\right)\right]$, the approximation

$$\tilde{w} \approx \frac{1}{\sqrt{\frac{\tilde{E}_b}{2} + \tilde{E}_b^{\,2}\left(1-\frac{\tilde{f}^*}{2}\right)^2}}. \tag{A5}$$

Each model therefore shows a different behavior regarding the evolution of its width as a function of $\tilde{E}_b$. Moreover, according to the conservation of the integral of $\tilde{p}(\tilde{f})$, $\tilde{p}(\tilde{f})$ obtained by the harmonic model broadens compared to $\tilde{p}(\tilde{f})$ obtained by the Bell model. While the difference in behavior between the two models could suggest that it is possible to discriminate between them in order to choose the most suitable model for analyzing experimental data, we showed in Sec. II that this theoretical difference gets blurred when accounting for the presence of experimental error in the analyzed measurements.

2. Average force $\langle\tilde{f}\rangle$

When analyzing single-bond force measurements, some authors [11] consider the mean rupture force rather than the most likely. We have calculated the average force $\langle\tilde{f}\rangle$ in both the Bell model and the harmonic model in order to compare it to $\tilde{f}^*$. In the Bell model, it is easy to compute the difference $\langle\tilde{f}\rangle - \tilde{f}^*$:

$$\langle\tilde{f}\rangle - \tilde{f}^* = \frac{\tilde{p}(\tilde{f}^*)}{\tilde{E}_b^{\,2}} \int_{-\tilde{E}_b\tilde{f}^*}^{+\infty} \alpha \exp(\alpha - e^{\alpha} + 1) d\alpha. \tag{A6}$$

Hence using Eq. (A1) which gives $\tilde{p}(\tilde{f})$, and provided that $\tilde{f}^*$ is sufficiently high and that $\tilde{r} > \tilde{r}_m$ (where $\tilde{r}_m$ is the loading rate below which $\tilde{f}^* = 0$), one obtains

$$\langle\tilde{f}\rangle - \tilde{f}^* \approx -\frac{\gamma}{\tilde{E}_b} \approx -\frac{0.577}{\tilde{E}_b}, \tag{A7}$$

where γ is the Euler-Mascheroni constant. Considering variables with dimensions, one gets a difference which is independent of the barrier height:

TABLE II. Parameters obtained for the Bell and the harmonic models by fitting data from Chen and Springer [1] after having set a value for t_D in the first column.

t_D (s)	x_b^{Bell} (nm)	x_b^{harm} (nm)	E_b^{Bell} (units of k_BT)	E_b^{harm} (units of k_BT)
10^{-11}	6.6×10^{-2}	7.0×10^{-2}	25.4	25.5
10^{-10}	6.6×10^{-2}	7.0×10^{-2}	23.1	23.2
10^{-9}	6.6×10^{-2}	7.1×10^{-2}	20.8	20.9

$$\langle f\rangle - f^* \approx -\frac{E_b}{x_b}\frac{\gamma}{\frac{E_b}{k_BT}} \approx -0.577\frac{k_BT}{x_b}. \tag{A8}$$

That is to say that for the above-mentioned conditions ($\tilde{f}^*$ and $\tilde{r}$ sufficiently high), the difference between $\langle f\rangle$ and f^* is independent of the loading rate. As an example, for a typical value x_b=0.5 nm, one gets $\langle f\rangle - f^* \approx -5$ pN. In the case of the harmonic model, we computed numerically $\langle \tilde{f}\rangle$ as a function of the loading rate for different energy barrier heights; in this model the difference is the mean and the most likely rupture force is a slowly varying function of $\ln \tilde{r}$, and, without details of the numerical study of its dependency of $\tilde{E}_b$, it led us to the conclusion that it could be reasonably considered as constant from an experimental point of view. As for w, the experimental error will modify the measured value of $\langle \tilde{f}\rangle$ and make it difficult to obtain information on the energy landscape with this parameter.

3. Maximum of the rupture force distribution, $p(f^*)$

The Bell model and the harmonic model exhibit a different evolution of $p(f^*)$ as a function of the loading rate. By using Eq. (A1) and the expression $\tilde{r}_m = \frac{\exp(-\tilde{E}_b)}{\tilde{E}_b}$, one obtains for the Bell model (with nondimensional variables)

$$\tilde{p}(\tilde{f}^*) = \tilde{E}_b \exp\left(\frac{\tilde{r}_m}{\tilde{r}} - 1\right), \tag{A9}$$

which tends to a constant value $\frac{1}{e}\tilde{E}_b$ as the loading rate tends towards infinity [back to dimensional variables, $p(f^*)$ tends toward $\frac{1}{e}\frac{x_b}{k_BT}$ as r tends towards infinity].

For the harmonic model, by injecting in the nondimensional version of Eq. (6) the explicit expression of $k_{off}(\tilde{f}^*)$, one obtains $\frac{1}{\tilde{r}}\exp\left[-\tilde{E}_b\left(1-\frac{\tilde{f}^*}{2}\right)^2\right] = \tilde{E}_b\left(1-\frac{\tilde{f}^*}{2}\right)$. Using this equality in the expression of $\tilde{p}(\tilde{f}^*)$ that is obtained from Eq. (A3), one obtains

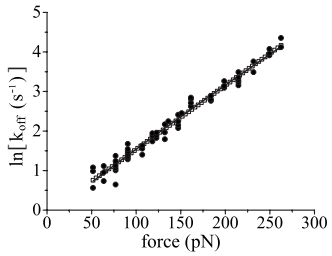

FIG. 12. Plot of the logarithm of the off-rate vs the applied force on a single bond between a single selectin and its ligand. Solid circles are taken from [1]. The solid line represents $\ln k_{off}$ fitted to the Bell model. The open squares represent $\ln k_{off}$ fitted to the harmonic model. Both fits are in excellent agreement, as well as the obtained parameters (see Table II).

$$\tilde{p}(\tilde{f}^*) = \tilde{E}_b\left(1-\frac{\tilde{f}^*}{2}\right)\exp\left(\sqrt{\pi\tilde{E}_b}\left(1-\frac{\tilde{f}^*}{2}\right)\exp\left[\tilde{E}_b\left(1-\frac{\tilde{f}^*}{2}\right)^2\right]\times\left\{\mathrm{erf}\left[\sqrt{\tilde{E}_b}\left(1-\frac{\tilde{f}^*}{2}\right)\right]-\mathrm{erf}\left(\sqrt{\tilde{E}_b}\right)\right\}\right). \tag{A10}$$

For $\tilde{r}$ sufficiently high, the exponential factor in the above expression tends towards a constant value, and $\tilde{p}(\tilde{f}^*) \sim 0.4\tilde{E}_b\left(1-\frac{\tilde{f}^*}{2}\right)$, that is to say that $\tilde{p}(\tilde{f}^*)$ is linearly decreasing with $\ln \tilde{r}$, for sufficiently high $\tilde{r}$ [with dimensional values, $p(f^*)$ will as a result be linearly decreasing with $\ln r$, for sufficiently high r]. These two different behaviors are illustrated in the example in Fig. 4(a).

APPENDIX B: EXPERIMENTS UNDER CONSTANT FORCE: EXAMPLE OF THE INTERACTION BETWEEN THE *L*-SELECTIN AND ITS LIGAND

Chen and Springer [1] compared several models describing the unbinding rate $k_{off}(f)$ of a single bond under a constant force f. The study was performed on the bond between *L*-selectin and its ligand. When considering a constant force f applied to a bond, the probability of the (slip-)bond to survive up to a time t is exponentially decreasing with t. The time constant of the decrease is the lifetime of the bond under force f, $\tau(f) = \frac{1}{k_{off}(f)}$.

In Ref. [1], the authors compared five models and concluded that among them, the Bell model fit the data significantly the best. By now using the harmonic model to fit their experimental data, we obtained a very close result to the one obtained with the Bell model, and close parameters for the energy barrier (see Fig. 12). Generally, these parameters depend on the value of t_D, so we considered values ranging from 10^{-11} to 10^{-9} s. They are shown in Table II. The relative error between both models is lower than 7% for x_b, and lower that 1% for E_b. This confirms that, as expected from Sec. II, both the Bell and harmonic models can be equivalently used and lead to similar results.

[1] S. Q. Chen and T. A. Springer, Proc. Natl. Acad. Sci. U.S.A. **98**, 950 (2001).
[2] A. Pierres, Biophys. J. **82**, 3214 (2002).
[3] E. L. Florin, V. T. Moy, and H. E. Gaub, Science **264**, 415 (1994).
[4] C. K. Lee *et al.*, Micron **38**, 446 (2007).
[5] E. Evans *et al.*, Proc. Natl. Acad. Sci. U.S.A. **101**, 11281 (2004).
[6] E. A. Evans and D. A. Calderwood, Science **316**, 1148 (2007).
[7] R. Merkel *et al.*, Nature (London) **397**, 50 (1999).
[8] F. Pincet and J. Husson, Biophys. J. **89**, 4374 (2005).
[9] S. C. Kuo and M. P. Sheetz, Science **260**, 232 (1993).
[10] A. L. Stout, Biophys. J. **80**, 2976 (2001).
[11] D. F. J. Tees, R. E. Waugh, and D. A. Hammer, Biophys. J. **80**, 668 (2001).
[12] P. Hanggi, P. Talkner, and M. Borkovec, Rev. Mod. Phys. **62**, 251 (1990).
[13] H. A. Kramers, Physica (Utrecht) **7**, 284 (1940).
[14] E. Evans, Annu. Rev. Biophys. Biomol. Struct. **30**, 105 (2001).
[15] E. Evans and P. M. Williams, in *Physics of Bio-Molecules and Cells*, edited by F. Julicher, P. Ormos, F. David, and H. Flyvbjerg (Springer-Verlag, Berlin, Germany, 2002), p. 145.
[16] G. I. Bell, Science **200**, 618 (1978).
[17] O. K. Dudko *et al.*, Proc. Natl. Acad. Sci. U.S.A. **100**, 11378 (2003).
[18] U. Seifert, Europhys. Lett. **58**, 792 (2002).
[19] H. Grubmuller, B. Heymann, and P. Tavan, Science **271**, 997 (1996).
[20] S. Izrailev *et al.*, Biophys. J. **72**, 1568 (1997).
[21] S. J. Marrink *et al.*, Biophys. J. **74**, 931 (1998).
[22] M. Evstigneev and P. Reimann, Phys. Rev. E **68**, 045103 (2003).
[23] Y. V. Pereverzev and O. V. Prezhdo, Phys. Rev. E **75**, 011905 (2007).
[24] E. Evans and K. Ritchie, Biophys. J. **72**, 1541 (1997).
[25] B. Heymann and H. Grubmuller, Phys. Rev. Lett. **84**, 6126 (2000).
[26] G. Hummer and A. Szabo, Proc. Natl. Acad. Sci. U.S.A. **98**, 3658 (2001).
[27] C. Jarzynski, Phys. Rev. Lett. **78**, 2690 (1997).
[28] C. Hyeon and D. Thirumalai, J. Phys.: Condens. Matter **19**, 113101 (2007).
[29] V. Barsegov and D. Thirumalai, J. Phys. Chem. B **110**, 26403 (2006).
[30] D. Bartolo, I. Derenyi, and A. Ajdari, Phys. Rev. E **65**, 051910 (2002).
[31] J. Z. Lou and C. Zhu, Biophys. J. **92**, 1471 (2007).
[32] Y. V. Pereverzev and O. V. Prezhdo, Phys. Rev. E **73**, 050902 (2006).
[33] F. Liu and Z. C. Ou-Yang, Phys. Rev. E **74**, 051904 (2006).
[34] M. Raible and P. Reimann, Europhys. Lett. **73**, 628 (2006).
[35] E. Evans and K. Ritchie, Biophys. J. **76**, 2439 (1999).
[36] G. Hummer and A. Szabo, Biophys. J. **85**, 5 (2003).
[37] H. Karcher *et al.*, Biophys. J. **90**, 2686 (2006).
[38] F. Hanke and H. J. Kreuzer, Phys. Rev. E **74**, 031909 (2006).
[39] H. J. Lin *et al.*, Phys. Rev. Lett. **98**, 088304 (2007).
[40] O. K. Dudko, G. Hummer, and A. Szabo, Phys. Rev. Lett. **96**, 108101 (2006).
[41] E. Perret, Proc. Natl. Acad. Sci. U.S.A. **101**, 16472 (2004).
[42] I. Derenyi, D. Bartolo, and A. Ajdari, Biophys. J. **86**, 1263 (2004).